01 Jan 2022

# Spatial Transformation of a Layer-To-Layer Control Model for Selective Laser Melting

Xin Wang

Robert G. Landers
*Missouri University of Science and Technology*, landersr@mst.edu

Douglas A. Bristow
*Missouri University of Science and Technology*, dbristow@mst.edu



## Recommended Citation

X. Wang et al., "Spatial Transformation of a Layer-To-Layer Control Model for Selective Laser Melting," *Proceedings of the American Control Conference*, pp. 2886 - 2891, Institute of Electrical and Electronics Engineers, Jan 2022.
The definitive version is available at https://doi.org/10.23919/ACC53348.2022.9867850

2022 American Control Conference (ACC)
Atlanta, USA, June 8-10, 2022

# A Spatial Transformation of a Layer-to-Layer Control Model for Selective Laser Melting

Xin Wang[1], Robert G. Landers[2], Douglas A. Bristow[1]

*Abstract*— **Selective Laser Melting (SLM) is an Additive Manufacturing (AM) technique with challenges in its complexity of process parameters and lack of control schemes. Traditionally, people tried time-domain or frequency-domain control methods, but the complexity of the process goes beyond these methods. In this paper, a novel spatial transformation of SLM models is proposed, which transforms the time-domain process into a spatial domain model and, thus, allows for state-space layer-to-layer control methods. In a space domain, this also provides the convenience of modelling laser path changes. Finally, a layer-to-layer Iterative Learning Control (ILC) method is designed and demonstrates the methodology of spatial control for SLM. A simulation demonstrates its application and performance.**

## I. Introduction

Additive Manufacturing (AM) is a fast-developing technique of huge interest. The attractive feature of AM is the capability of manufacturing complex geometries and the reduction of wastes. Powder Bed Fusion (PBF) is one of AM techniques with a relatively high geometry accuracy. In spite of much effort devoted to PBF for nearly half a century, PBF is still not widely adopted by many industry sectors [1]. Two big challenges of PBF are repeatability and controllability of the process.

Selective Laser Melting (SLM) is one of PBF techniques, which fuses and solidifies selected regions of powder into solid parts layer by layer. Just like other AM techniques, due to the lack of quality assurance in open loop systems, researchers devoted much effort to the study of monitoring, modelling and control of the process, including but not limited to SLM.

The SLM process and its monitoring and control are illustrated in Figure 1. The three figures (a), (b) and (c) represent three aspects that different researchers pay attention to. Figure 1 (a) represents the area of control and monitoring. People install optical sensors in SLM systems to collect melt pool data for feedback control. In monitoring and control, Hu et al. [2] used a coaxial infrared camera to capture images of melt pools, and they monitored temporal signals of melt pool pixel numbers and tried to control the system based on the melt pool features. Kruth [3-7] et al. also captured melt pool images using a thermal camera, monitored defects and tried PID control using temporal signals and tried modelling it in a frequency domain. Demir et al. (2018) [8] used optical sensors with multiple channels of bandwidths to record temporal signals of image radiation and its statistics. Shkoruta et. al [9-10] used IR temporal signals for Iterative Learning Control (ILC) and also for frequency-domain system identification, respectively. Most of the work above concentrates on the time-domain dynamics. System identification and control in time and frequency domains are well proven techniques, but they show their weakness in SLM for the following reasons:

(1) The SLM process is very fast and transient, and the bandwidths of a control system may not allow a fast reaction to laser activities. It is difficult to transplant temporal or frequency domain control into SLM from other AM techniques, like Laser Metal Deposition (LMD).

(2) In SLM, the laser path is variant, and this is necessary for better homogeneity of fabrications. However, temporal signals alone cannot provide location information without path information.

(3) Traditional temporal or frequency analyses often do not take the layer-to-layer dynamics into consideration.

Therefore, it is necessary to solve the SLM control problem beyond the perspective of temporal modelling.

On the other side, Figure 1 (b) represents the concern of manufacturing researchers, who are more interested in non-destructive quality monitoring of SLM. In manufacturing, melt pool data are processed into spatial feature maps so that defects can be located. Renken et. al (2018) generated spatial color maps from temporal signals of a pyrometer [13]. Krauss et al. [14-15] presented more detailed work on visualized spatial feature maps of PBF. Lough et. al [16-17] studied the correlation between IR feature spatial maps, microdefects and engineering properties, which demonstrated IR camera imaging as a tool for defect locating and quality prediction. From the spatial perspective, researchers process data of AM in a spatial domain and render more convenience in identifying local defects and the potentiality of local quality control.

Since manufacturing researchers in SLM have been devoted to establishing a knowledge base of spatial features and defect detection, and layerwise control is more suitable for SLM, control researchers began to design layer-to-layer control in a state-space and spatial domain. Spector et al. [18] proposed a simplified and fast control-oriented model and designed layer-to-layer control. Lately, Yavari and Cole et al. [19-22] proposed a model that meshed a part into spatial nodes and borrowed the concept of the Laplacian matrix from

X. Wang and D. A. Bristow are with Missouri University of Science and Technology, Mechanical Engineering Department, Rolla, MO 65409, USA (e-mails: {xwc9c, dbristow}@mst.edu).

R. G. Landers is with University of Notre Dame, Aerospace and Mechanical Engineering, South Bend, Indiana 46556-4634, USA (e-mail: rlanders@nd.edu).



978-1-6654-5196-3/$31.00 ©2022 AACC

graph theory to represent the nodal connections in geometries. Wang et al. built a formulaic framework of spatial models [24-25], which is the antecedent of this paper.

In this paper, a novel control-oriented model is proposed, which is a bridge between temporal models and spatial models, and Figure 1 (c) is complemented so that a complete model for SLM is formulated mathematically. The flowchart will be fulfilled mathematically in the following sections. It lays the basis of layer-to-layer control design. In this paper, a model is constructed by steps from the fundamental heat transfer law and it is the synthesis of three critical factors (geometry, laser power and path) of SLM. It leads to the idea of spatial monitoring and layerwise control, and it leaves a wide space in future for other advanced modelling and system identification techniques.

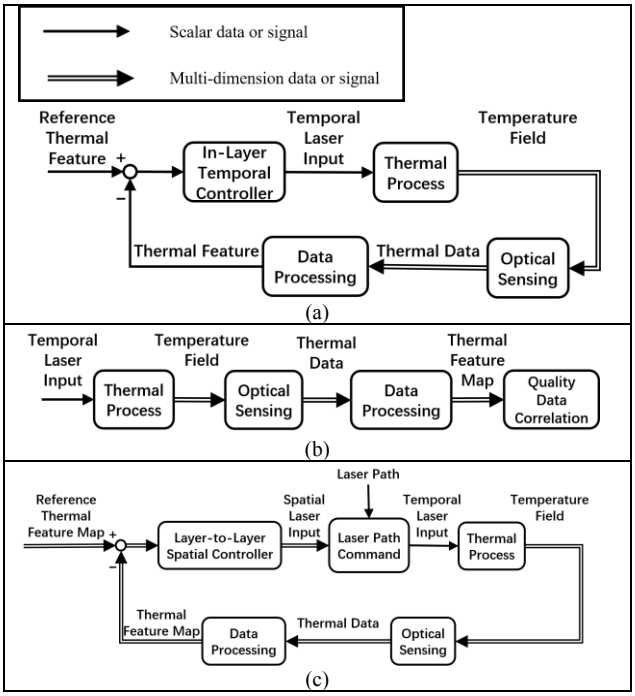


Figure 1: SLM Process in Control and Manufacturing (a) Traditional SLM Control (b) Melt Pool Monitoring in SLM Manufacturing (c) Layer-to-Layer Spatial Control of SLM

## II. Spatial Dynamic Model for SLM

### A. Finite Difference Model of SLM

Selective laser melting is a complex synthesis of many physical processes, involving heat conduction, convection, radiation, phase transition and vaporization. For a practical purpose of modelling and control, some assumptions are made:

(1) The dominant heat transfer mode is heat conduction, while convection and radiation are ignored.

(2) The status (solid or powder) of an element is represented by its conductivity and diffusivity.

(3) For each iteration, the laser path and the laser power are known.

(4) The substrate temperature is set to be 0 by shifting all temperature by the ambient temperature.

The heat conduction law, namely, the Fourier-Biot equation, is

$$\mathbf{\Delta} T + \frac{q}{k_c} = \frac{1}{\alpha}\frac{\partial T}{\partial t}, \tag{1}$$

where $\mathbf{\Delta}$ is the Laplacian operator, $T$ (K) is the temperature field, $q$ (W/m$^3$) is the heat power per volume, $k_c$ (W/(m·K)) is the conductivity and $\alpha$ (m$^2$/s) is the diffusivity. The finite difference form of the Fourier-Biot equation is

$$\begin{aligned}&\frac{T_{d_1+1,d_2,d_3}(n)+T_{d_1-1,d_2,d_3}(n)-2T_{d_1,d_2,d_3}(n)}{\Delta x^2}\\&+\frac{T_{d_1,d_2+1,d_3}(n)+T_{d_1,d_2-1,d_3}(n)-2T_{d_1,d_2,d_3}(n)}{\Delta y^2}\\&+\frac{T_{d_1,d_2,d_3+1}(n)+T_{d_1,d_2,d_3-1}(n)-2T_{d_1,d_2,d_3}(n)}{\Delta z^2}\\&+\frac{q_{d_1,d_2,d_3}(n+1)}{k_c}=\frac{T_{d_1,d_2,d_3}(n+1)-T_{d_1,d_2,d_3}(n)}{\alpha\Delta t},\end{aligned} \tag{2}$$

where ($d_1$, $d_2$, $d_3$) is the 3D index of a block, $n$ is the time index and $\Delta t$ (s) is the time step length. The domain is illustrated in Figure 2. Not all elements are solid parts. Some of the elements are steel and some are loose powder.

In Figure 2, the size of a block is given such that $\Delta x$ is the laser pulse distance, $\Delta y$ is the hatch spacing, and $\Delta z$ is the layer thickness. Therefore, each meshing block contains one laser pulse and one sample, namely,

$$\Delta x = V\Delta t, \tag{3}$$

where $V$ is the laser velocity. In practice, the sample locations may not match with the blocks. If so, interpolation or down-sample can be applied to create sample points matching with the grid.

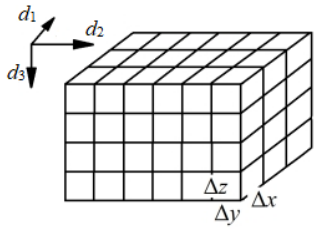


Figure 2: Domain of the Finite Difference Model

### B. Definitions of State-Space Variables

Before the introduction of state-space variables, the indices of elements are vectorized. The vectorized powder bed model is shown in Figure 3, where there are $L$ layers, and each layer contains $m$×$p$ blocks. The 3D spatial indices ($d_1$, $d_2$, $d_3$) are mapped into a scalar index $v$ by $f$: $\mathbb{R}^3 \to \mathbb{R}$

$$v = f(d_1,d_2,d_3) = d_1 + (d_2-1)p + (d_3-1)mp. \tag{4}$$

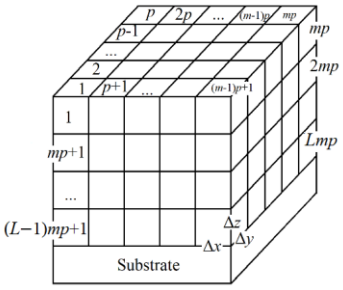


Figure 3: Vectorized Numbering of Elements in SLM Model

With the finite difference model, the state-space variables are to be introduced. The temperature $T$ of an element is denoted by a state $x_v$. For layer-to-layer control, an iteration number $l$ is added to the arguments so that $(n)$ is augmented to $(n, l)$. Then the vectorization from $T$ to $\mathbf{x}$ is

$$x_{f(d_1,d_2,d_3)}(n,l) = T_{d_1,d_2,d_3}(n,l), \tag{5}$$

where $(n, l)$ is the $n^{\text{th}}$ time step of the $l^{\text{th}}$ iteration. In this way, the state vector for the whole system at the end of the $n^{\text{th}}$ pulse during the $l^{\text{th}}$ iteration is

$$\begin{aligned}\mathbf{x}(n,l) &= \left[x_1(n,l) \quad x_2(n,l) \quad \cdots \quad x_{pmL}(n,l)\right]^{\mathrm{T}} \\ &= \left[T_{1,1,1}(n,l) \quad T_{2,1,1}(n,l) \quad \cdots \quad T_{p,m,L}(n,l)\right]^{\mathrm{T}}.\end{aligned} \tag{6}$$

As a remark, $l$ is the iteration number of layer processing and $L$ is total number of layers included in the model, which are different concepts, because sometimes only a limited number of top layers are considered in a model for simplicity.

The input power per volume dimensionalized into K is defined as

$$u_{f(d_1,d_2,1)}(n,l) = \frac{\alpha\Delta t}{k_c} q_{d_1,d_2,1}(n,l), \tag{7}$$

and the input vector of the system is

$$\begin{aligned}\mathbf{u}(n,l) &= \left[u_1(n,l) \quad u_2(n,l) \quad \cdots \quad u_{pm}(n,l)\right]^{T} \\ &= \frac{\alpha\Delta t}{k_c}\left[q_{1,1,1}(n,l) \quad q_{2,1,1}(n,l) \quad \cdots \quad q_{p,m,1}(n,l)\right]^{\mathrm{T}}.\end{aligned} \tag{8}$$

To separate spatial information and temporal information, the spatial mapping of the input is defined as

$$\mathbf{u}_{\mathrm{s}}(l) = \left[u_{\mathrm{s},1}(l) \quad u_{\mathrm{s},2}(l) \quad \cdots \quad u_{\mathrm{s},mp}(l)\right]^{T}, \tag{9}$$

where $u_{\mathrm{s},v}$ is the amplitude of the pulse at the element index $v$, namely the amplitude of $u_v$. In this way, the vector $\mathbf{u}_{\mathrm{s}}$ is only the spatial information of the laser. The laser power sequence along the time is

$$\mathbf{u}_{\mathrm{t}}(l) = \left[u_{\mathrm{t},1}(l) \quad u_{\mathrm{t},2}(l) \quad \cdots \quad u_{\mathrm{t},mp}(l)\right]^{T}, \tag{10}$$

where $u_{\mathrm{t},w}$ is the power at the $w^{\text{th}}$ step. Now 3 types of input definitions are introduced, and researchers may use different ones. To eliminate the ambiguity, an example is shown.

**Example 1 (Input Definitions):** Consider a system with only 4 elements in Figure 4. The laser follows the element index ($v$) $1 \rightarrow 2 \rightarrow 4 \rightarrow 3$ with dimensionalized input power $0.4 \rightarrow 0.5 \rightarrow 0.6 \rightarrow 0.7$ ($\times 10^4$ K) in the $l^{\text{th}}$ iteration. Then the system input vectors are

$$\begin{cases}\mathbf{u}(1,l) = \left[0.4 \quad 0 \quad 0 \quad 0\right]^{\mathrm{T}} \\ \mathbf{u}(2,l) = \left[0 \quad 0.5 \quad 0 \quad 0\right]^{\mathrm{T}} \\ \mathbf{u}(3,l) = \left[0 \quad 0 \quad 0 \quad 0.6\right]^{\mathrm{T}} \\ \mathbf{u}(4,l) = \left[0 \quad 0 \quad 0.7 \quad 0\right]^{\mathrm{T}}\end{cases}. \tag{11}$$

The spatial input is

$$\mathbf{u}_{\mathrm{s}}(l) = \left[0.4 \quad 0.5 \quad 0.7 \quad 0.6\right]^{\mathrm{T}}. \tag{12}$$

The temporal input is

$$\mathbf{u}_{\mathrm{t}}(l) = \left[0.4 \quad 0.5 \quad 0.6 \quad 0.7\right]^{\mathrm{T}}. \tag{13}$$

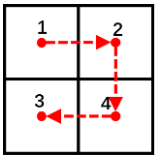


Figure 4: Example of a 4-Element System

These 3 types of input definitions have different applications:

(a) A system input is used for state-space matrix equations.

(b) A spatial input is used for spatial control (See the next section).

(c) A temporal input is used for laser power commands and traditional control of SLM.

The spatial input vector and the temporal input vector have different index systems. The laser path transform matrix for the top layer is defined as following:

$$\mathbf{P}_{\mathrm{y}} = \left[\mathbf{p}_1 \quad \mathbf{p}_2 \quad \cdots \quad \mathbf{p}_{mp}\right]^{T}, \tag{14}$$

where

$$\mathbf{p}_w = \left[0 \quad \cdots \quad 0 \quad 1 \quad 0 \quad \cdots \quad 0\right]^{T}, \tag{15}$$

where $w$ is the pulse step index along the path and 1 is placed at its location $v$. Using this definition, the relationship between the temporal input signal and the spatial input map is

$$\mathbf{u}_{\mathrm{t}} = \mathbf{P}_{\mathrm{y}}\mathbf{u}_{\mathrm{s}}. \tag{16}$$

**Example 2 (Laser Path Transform Matrix)**: In Example 1, the transform matrix between spatial and temporal inputs is

$$\mathbf{P}_{\mathrm{y}} = \begin{bmatrix}1 & 0 & 0 & 0 \\ 0 & 1 & 0 & 0 \\ 0 & 0 & 0 & 1 \\ 0 & 0 & 1 & 0\end{bmatrix}. \tag{17}$$

A temporal output is a measurement of the surface states

$$\mathbf{y}_{\mathrm{t}}(l)=\begin{bmatrix} y_{\mathrm{t},1}(l) & y_{\mathrm{t},2}(l) & \cdots & y_{\mathrm{t},mp}(l)\end{bmatrix}^{T}, \quad (18)$$

where

$$y_{\mathrm{t},w}(l)=f_M\left(x_1(w,l),x_2(w,l),\cdots,x_{mp}(w,l)\right), \quad (19)$$

where $f_M$ may be any measurement function. The spatial output is

$$\mathbf{y}_{\mathrm{s}}=\mathbf{P}_{\mathrm{y}}^{-1}\mathbf{y}_{\mathrm{t}}. \quad (20)$$

If the output is a linear combination of the states, then $\mathbf{e}_w$ is the linear sampling operator, yielding

$$y_{\mathrm{t},w}(l)=\mathbf{e}_w^{\mathrm{T}}\mathbf{x}(w,l). \quad (21)$$

**Example 3 (Linear Sampling Operator):** Consider the max temperature

$$y_{\mathrm{t},w}(l)=\max_{1\le v\le mp}\left\{x_v(w,l)\right\}, \quad (22)$$

which is often used in SLM monitoring. For simplification, assume that the maximal temperature in an image is just at the laser point. The estimate of maximal temperature in an image is

$$y_{\mathrm{t},w}(l)\approx x_{v_L(w)}(w,l), \quad (23)$$

where $v_L(w)$ is the laser position at the time step $w$. Then the linear sampling operator is

$$\mathbf{e}_w=\begin{bmatrix}\mathbf{p}_w^{\mathrm{T}} & \mathbf{0}^{\mathrm{T}}\end{bmatrix}^{\mathrm{T}}. \quad (24)$$

Consider another measurement of the sum of surface temperature

$$y_{\mathrm{t},w}(l)=\sum_{v=1}^{mp}x_v(w,l). \quad (25)$$

Then the linear sampling operator is

$$\mathbf{e}_w=\begin{bmatrix}\mathbf{1}_{1\times mp} & \mathbf{0}_{1\times(L-1)mp}\end{bmatrix}^{\mathrm{T}}. \quad (26)$$

*C. Summary of Temporal and Spatial Models*

From Eq. (2), the finite difference form of heat conduction equation is [24]

$$\mathbf{x}(n+1,l)=\mathbf{A}(l)\mathbf{x}(n,l)+\mathbf{B}(l)\mathbf{u}(n+1,l). \quad (27)$$

Assume that the initial state of each iteration is a constant 0. Then the input-output relation is

$$\mathbf{y}_{\mathrm{t}}(l)=\mathbf{G}_{\mathrm{t}}(l)\mathbf{u}_{\mathrm{t}}(l), \quad (28)$$

$$\mathbf{G}_{\mathrm{t}}=\begin{bmatrix} g_{11} & \cdots & g_{1N}\\ \vdots & & \vdots\\ g_{N1} & \cdots & g_{NN}\end{bmatrix}. \quad (29)$$

It can be derived from Eq. (2) with zero initial states that

$$g_{ij}=\begin{cases}\mathbf{e}_i^{\mathrm{T}}\mathbf{A}^{i-j}\mathbf{B}\mathbf{p}_j, i-j\ge 0\\ 0, i-j<0\end{cases}. \quad (30)$$

If the input-output relation is transformed into the spatial domain, then

$$\mathbf{y}_{\mathrm{s}}=\mathbf{G}_{\mathrm{s}}\mathbf{u}_{\mathrm{s}}, \quad (31)$$

$$\mathbf{G}_{\mathrm{s}}=\mathbf{P}_{\mathrm{y}}^{-1}\mathbf{G}_{\mathrm{t}}\mathbf{P}_{\mathrm{y}}. \quad (32)$$

Now the concepts at the beginning in Figure 1 are fulfilled in Figure 5. Traditionally, people tried to identify, model and control SLM systems in a time domain (or frequency domain), but the effect of laser path is difficult to be integrated into a model explicitly. In path-variant cases, a spatial model is preferred for these reasons:

(a) In applications of SLM, where defects appear is more important than when defects appear.

(b) The spatial model takes the laser path into consideration.

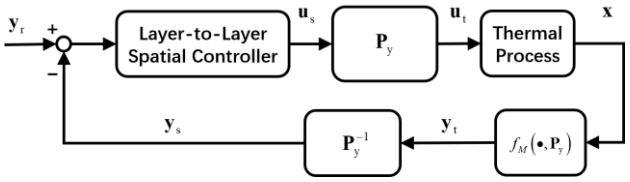


Figure 5: Relation Between Temporal Model and Spatial Model

## III. Layer-to-Layer Control Design: An Example

### *A. Path-Dependency of Matrix* **G**

The input-output relation of the system is given by Eq. (30), where **e** and **p** are operators representing the laser path, and **A** and **B** are system matrices only dependent on geometry. The two factors, path and geometry, are separable. Although **A** and **B** are hard to estimate due to the nonlinearity in the real world, the path factors are absolutely known. For simplicity, a linear model is assumed in this paper.

**Example 4 (Path Dependency of Spatial Output Maps)** Consider the geometry in Figure 6, with a size of 40 × 80 × 10 elements. The element size is 50 μm × 50 μm × 50 μm. The conductivity and diffusivity are $k_c$ = 300 W/(m·K) and $\alpha$ = 5.1 ×10$^{-5}$ m$^2$/s, respectively. The input power is 200 W constantly. For simplicity of the model, the peak temperature is chosen as the output. The output temperature unit is K. For simplicity, a linear model is used for simulation. The output maps and temporal signals from the simulation are shown in Figure 7 and Figure 8.

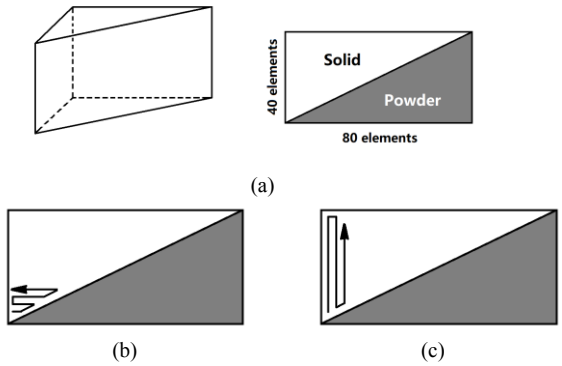


Figure 6: Simulation Case (a) Layer Geometry (b) Path 1 (c) Path 2

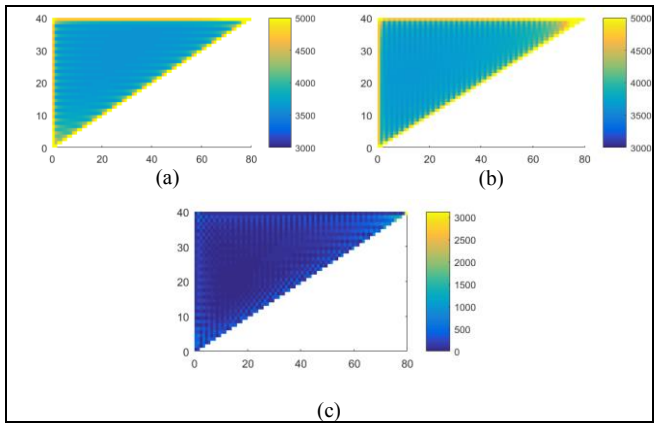


Figure 7: Simulation of Spatial Output from Constant Input (a) Output of Path 1 (b) Output of Path 2 (c) Absolute Difference Between (a)(b)

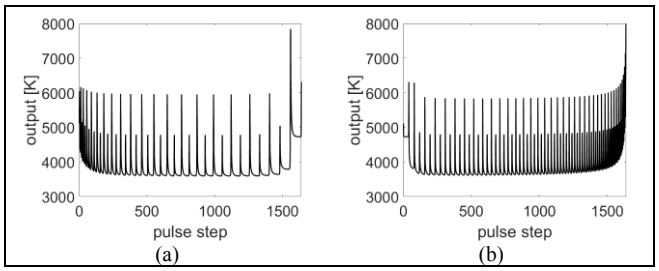


Figure 8: Simulation of Temporal Output from Constant Input (a) Output of Path 1 (b) Output of Path 2

In addition to the geometry effect, the laser path effect is also illustrated. Path 2 has a greater output at the upper-right corner than Path 1, because in Path 2 the laser stays persistently in the corner region for a longer time. Although the simulation model is linear and it is an ideal case of heat conduction, it illustrates the critical influential factors in SLM.

*B. Layer-to-Layer SLM Control*

Typically, Iterative Learning Control (ILC) solves a repeatable control problem in the form

$$\mathbf{y}_s(l) = \mathbf{G}_s \mathbf{u}_s(l), \tag{33}$$

$$\mathbf{u}_s(l+1) = \mathbf{u}_s(l) + \mathbf{\Gamma} \mathbf{e}_s(l), \tag{34}$$

$$\mathbf{e}_s(l) = \mathbf{y}_r - \mathbf{y}_s(l), \tag{35}$$

where $\mathbf{y}_r$ is the reference output. The convergence condition is

$$\left\| \mathbf{I} - \mathbf{G}_s \mathbf{\Gamma} \right\| < 1, \tag{36}$$

However, $\mathbf{G}_s$ is variant when the path changes. To solve this problem, assume that there exists an estimate $\hat{\mathbf{G}}_s$ of the system $\mathbf{G}_s$. A control law is

$$\mathbf{u}_s(l+1) = \mathbf{Q}(l)\left[\mathbf{u}_s(l) + \mathbf{\Gamma} \mathbf{e}_s(l)\right], \tag{37}$$

$$\mathbf{Q}(l) = \hat{\mathbf{G}}_s^{-1}(l+1)\hat{\mathbf{G}}_s(l). \tag{38}$$

Suppose the estimate of $\mathbf{G}_s$ is bounded by

$$\left\| \mathbf{G}_s - \hat{\mathbf{G}}_s \right\| < \varepsilon. \tag{39}$$

Then

$$\left\| \mathbf{e}_s(l+1) \right\| \le \left\| \mathbf{I} - \hat{\mathbf{G}}_s(l)\mathbf{\Gamma} \right\| \left\| \mathbf{e}_s(l) \right\| + 2\varepsilon b_u, \tag{40}$$

$$\left\| \mathbf{e}_s(\infty) \right\| \le \frac{2\varepsilon b_u}{1-\rho}, \tag{41}$$

where

$$\rho = \max_l \left\| \mathbf{I} - \hat{\mathbf{G}}_s(l)\mathbf{\Gamma} \right\|, \tag{42}$$

$$\left\| \mathbf{u}_s \right\| \le b_u. \tag{43}$$

By adding an estimator, it is possible to correct the control law in the presence of system variance. To this point, a well-trained estimator $\hat{\mathbf{G}}_s$ is a prerequisite. Once an estimation of $\hat{\mathbf{G}}_s$ exists before applying ILC control, the boundedness of the estimator error implies the boundedness of the output error. The capability of the spatial modelling and layer-to-layer control relies on the performance of the estimation method.

**Example 5 (Control Simulation)**

Apply the control function in Eq. (37) to Example 4. The initial power is 200 W and the target reference output is 3600 K. The laser scan Path 1 and Path 2 are applied by turns. For simplicity and fast computation, a linear model is assumed and the output is the peak temperature.

When the two gains $\mathbf{G}_{s1}$ and $\mathbf{G}_{s2}$ are known without any error, the control simulation results are shown in Figure 9. At the beginning, a uniform input results in a non-uniform output. As the learning process proceeds, the input decreases at the previous hot positions, so Figure 9 (e) has a roughly inverse color of Figure 9 (b).

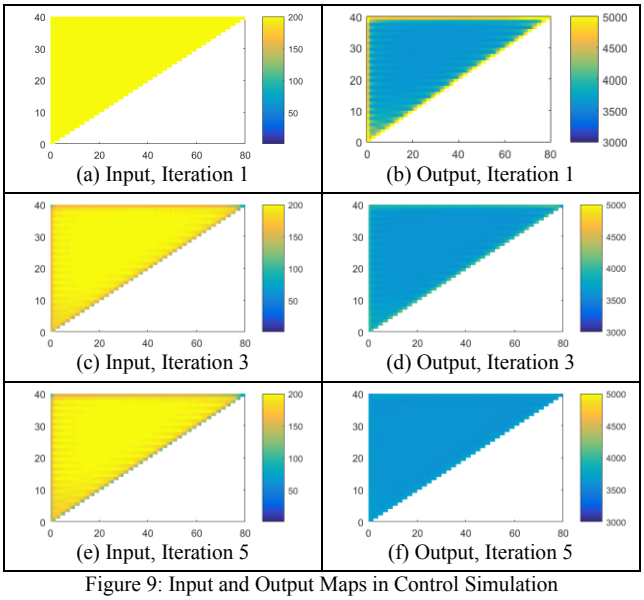


Figure 9: Input and Output Maps in Control Simulation

When the estimation errors of elements in $\mathbf{G}_s$ are simulated by evenly-distributed random errors with the ranges of 0%, ±5% and ±10% in each element of $\mathbf{G}_s$, the simulation results are in Figure 10. The performance depends on the accuracy of $\mathbf{G}_s$.

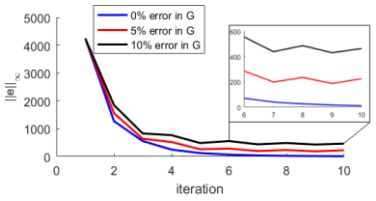


Figure 10: Error in the Control Simulation

## IV. Conclusions

In this paper, a novel spatial transformation of an SLM model is proposed as a bridge between spatial monitoring and temporal SLM control. Not only does the model include geometry dependency and path dependency explicitly, but also tries to design a layer-to-layer controller. Once an estimate of the system matrix exists, the control law can make the output error converge. A simulation demonstrates the spatial layer-to-layer control in the presence of path variance and its performance depends on the accuracy of the estimator.

## References


[1] Haghdadi, Nima, Majid Laleh, Maxwell Moyle, and Sophie Primig. "Additive manufacturing of steels: a review of achievements and challenges." Journal of Materials Science 56, no. 1 (2021): 64-107.

[2] Hu, Dongming, and Radovan Kovacevic. "Sensing, modeling and control for laser-based additive manufacturing." International Journal of Machine Tools and Manufacture 43, no. 1 (2003): 51-60.

[3] Kruth, Jean-Pierre, Peter Mercelis, Jonas Van Vaerenbergh, and Tom Craeghs. "Feedback control of selective laser melting." In Proceedings of the 3rd international conference on advanced research in virtual and rapid prototyping, pp. 521-527. Taylor & Francis Ltd, 2007.

[4] Berumen, Sebastian, Florian Bechmann, Stefan Lindner, Jean-Pierre Kruth, and Tom Craeghs. "Quality control of laser-and powder bed-based Additive Manufacturing (AM) technologies." Physics procedia 5 (2010): 617-622.

[5] Clijsters, Stijn, Tom Craeghs, Sam Buls, Karolien Kempen, and J-P. Kruth. "In situ quality control of the selective laser melting process using a high-speed, real-time melt pool monitoring system." The International Journal of Advanced Manufacturing Technology 75, no. 5-8 (2014): 1089-1101.

[6] Craeghs, Tom, Florian Bechmann, Sebastian Berumen, and Jean-Pierre Kruth. "Feedback control of Layerwise Laser Melting using optical sensors." Physics Procedia 5 (2010): 505-514.

[7] Berumen, Sebastian, Florian Bechmann, Stefan Lindner, Jean-Pierre Kruth, and Tom Craeghs. "Quality control of laser-and powder bed-based Additive Manufacturing (AM) technologies." Physics procedia 5 (2010): 617-622.

[8] Gökhan Demir, Ali, Chiara De Giorgi, and Barbara Previtali. "Design and implementation of a multisensor coaxial monitoring system with correction strategies for selective laser melting of a maraging steel." Journal of Manufacturing Science and Engineering 140, no. 4 (2018).

[9] Shkoruta, Aleksandr, William Caynoski, Sandipan Mishra, and Stephen Rock. "Iterative learning control for power profile shaping in selective laser melting." In 2019 IEEE 15th International Conference on Automation Science and Engineering (CASE), pp. 655-660. IEEE, 2019.

[10] Shkoruta, Aleksandr, Sandipan Mishra, and Stephen Rock. "An experimental study on process modeling for selective laser melting." In 2020 American Control Conference (ACC), pp. 467-473. IEEE, 2020.

[11] Tang, Lie, and Robert G. Landers. "Melt pool temperature control for laser metal deposition processes—Part I: Online temperature control." Journal of manufacturing science and engineering 132, no. 1 (2010).

[12] Liu, Yangbo, Liuping Wang, and Milan Brandt. "Model predictive control of laser metal deposition." The International Journal of Advanced Manufacturing Technology 105, no. 1 (2019): 1055-1067.

[13] Renken, Volker, Lutz Lübbert, Hendrik Blom, Axel von Freyberg, and Andreas Fischer. "Model assisted closed-loop control strategy for selective laser melting." Procedia CIRP 74 (2018): 659-663.

[14] Krauss, Harald, Thomas Zeugner, and Michael F. Zaeh. "Layerwise monitoring of the selective laser melting process by thermography." Physics Procedia 56 (2014): 64-71.

[15] Krauss, Harald, Thomas Zeugner, and Michael F. Zaeh. "Thermographic process monitoring in powderbed based additive manufacturing." In AIP Conference Proceedings, vol. 1650, no. 1, pp. 177-183. American Institute of Physics, 2015.

[16] Lough, Cody S., Xin Wang, Christopher C. Smith, Robert G. Landers, Douglas A. Bristow, James A. Drallmeier, Ben Brown, and Edward C. Kinzel. "Correlation of SWIR imaging with LPBF 304L stainless steel part properties." Additive Manufacturing 35 (2020): 101359.

[17] Lough, Cody S., Xin Wang, Christopher C. Smith, Olaseni Adeniji, Robert G. Landers, Douglas A. Bristow, and Edward C. Kinzel. "Use of swir imaging to monitor layer-to-layer part quality during slm of 304l stainless steel." In Proceedings of the 29th Annual International Solid Freeform Fabrication Symposium, Austin, TX, USA, pp. 13-15. 2018.

[18] Spector, Michael JB, Yijie Guo, Souvik Roy, Max O. Bloomfield, Antoinette Maniatty, and Sandipan Mishra. "Passivity-based iterative learning control design for selective laser melting." In 2018 Annual American Control Conference (ACC), pp. 5618-5625. IEEE, 2018.

[19] Yavari, Reza, Richard Williams, Kevin Cole, Paul Hooper, and Prahalad Rao. "Thermal modeling in metal additive manufacturing using graph theory: Experimental validation with in-situ infrared thermography data from laser powder bed fusion." In International Manufacturing Science and Engineering Conference, vol. 84256, p. V001T01A028. American Society of Mechanical Engineers, 2020.

[20] Yavari, Reza, Kevin D. Cole, and Prahalad Rao. "A graph theoretic approach for near real-time prediction of part-level thermal history in metal additive manufacturing processes." In International Manufacturing Science and Engineering Conference, vol. 58745, p. V001T01A030. American Society of Mechanical Engineers, 2019.

[21] Yavari, M. Reza, Kevin D. Cole, and Prahalada Rao. "Thermal modeling in metal additive manufacturing using graph theory." Journal of Manufacturing Science and Engineering 141, no. 7 (2019): 071007.

[22] Cole, Kevin D., M. Reza Yavari, and Prahalada K. Rao. "Computational heat transfer with spectral graph theory: Quantitative verification." International Journal of Thermal Sciences 153 (2020): 106383.

[23] Tapia, Gustavo, and Alaa Elwany. "A review on process monitoring and control in metal-based additive manufacturing." Journal of Manufacturing Science and Engineering 136, no. 6 (2014).

[24] Wang, Xin, Cody S. Lough, Douglas A. Bristow, Robert G. Landers, and Edward C. Kinzel. "A Layer-to-layer Control-Oriented Model for Selective Laser Melting." In 2020 American Control Conference (ACC), pp. 481-486. IEEE, 2020.

[25] Wang, Xin, Douglas A. Bristow, and Robert G. Landers. "A Switched Adaptive Model for Layer-to-Layer Selective Laser Melting With Varying Laser Paths." In Dynamic Systems and Control Conference, vol. 84287, p. V002T24A002. American Society of Mechanical Engineers, 2020.